Grey wolf optimization algorithm-based robust neural learning control of passive torque simulators with predetermined performance

Seyyed Amirhossein SAADAT
amirhossein.saadat@yahoo.com

Mohammad Mehdi FATEH
mmfateh@shahroodut.ac.ir

Javad KEIGHOBADI
javad_keighobadi@yahoo.com

Grey wolf optimization algorithm-based robust neural learning control of passive torque simulators with predetermined performance

Seyyed Amirhossein SAADAT, Mohammad Mehdi FATEH, Javad KEIGHOBADI*

Shahrood University of Technology, Shahrood, Semnan, Iran

Abstract: In flight control systems, the actuators need to tolerate aerodynamic torques and continue their operations without interruption. To this end, using the simulators to test the actuators in conditions close to the real flight is efficient. On the other hand, achieving the guaranteed performance encounters some challenges and practical limitations such as unknown dynamics, external disturbances, and state constraints in reality. Thus, this article attempts to present a robust adaptive neural network learning controller equipped with a disturbance observer for passive torque simulators (PTS) with load torque constraints. The radial basis function networks (RBFNs) are employed to identify the unknown terms, providing information for the disturbance observer. Besides, the tuning parameters are chosen optimally by adopting the grey wolf optimization (GWO) algorithm. The closed-loop system stability is also proven by the barrier Lyapunov function (BLF) while the total uncertainties, including system dynamics, friction, and disturbance, are tracked by the total estimation. Thus, the predetermined performance, robust behavior, and high-precision estimation are the achievements of the presented controller for PTS. To confirm the ability of the proposed control idea, simulations are provided. Furthermore, a comparison scenario is also considered to emphasize the supremacy of the proposed control system.

Key words: Neural network, passive torque simulator, state constraint, disturbance observer, grey wolf optimization algorithm, robust control.

1. Introduction

In real flight, the actuators which control the surfaces, rotors, and the moving parts of plane fins are exposed to aerodynamic torques. The flight actuator system plays a key role in directing the flight equipment. Actuators need to tolerate such aerodynamic torques and continue their operations without interruption. In order to simulate real-world applications, the hardware in the loop (HIL) is a suitable solution since it may lead to reducing the time and costs, and also mitigating the risks arising from field experiments [1, 2]. This is a technique whereby real signals from the controller are synchronized with a test system simulating reality. Tests and designs are carried out as if they were in the real world, using an iteration system. The HIL is used in the academic research and technical fields, especially in the different dimensions of engineering, including aircraft and aerospace industries [3, 4], power systems [5, 6], vehicle systems [7, 8], marine systems [9], robotics [10, 11], telecommunications [12], and experimental mass and spring systems [13].

The PTS is one of the most important equipment in HIL systems, known as the aerodynamic load simulator, and is based on the terms and trajectory of the flight, the aerodynamic load torque, or the forces

---

*Correspondence: javad_keighobadi@yahoo.com

acting on the flight control system. Parameter uncertainties, extra torque, torque resulting from nonlinear friction, and disturbance are major factors affecting the performance of PTS that should be considered during the design procedure. Considering different challenges in the simulator and controller design leads to increasing the accuracy and efficiency of the designed system [14, 15].

Interesting and diverse research has been conducted with the use of aerodynamic load simulators based on torque control. In [16], an adaptive robust control law is derived to control an electrical load simulator in which an extended state observer is adopted to estimate the uncertainty. In [17], an actuator velocity input feedforward compensating method is proposed for an electro-hydraulic load simulator. In [18], a robust control approach considering nonlinearity and external active motion disturbance is utilized for a load simulator. In [19], a pitch control approach is suggested to reduce aerodynamic loads and torque ripples for wind turbines. In [20], an observer-based controller is employed for an electro-hydraulic load simulator using a dynamic surface approach and a synchronous compensation is adopted to remove the actuator's motion effects. In the framework of the feedback linearization control, a neural network (NN)-based inversion scheme is applied to a hydraulic actuator [21]. In [22], a torsion spring is designed by using the double torsion spring precompression method for a load simulator with zero compensation. In [23], a desired model compensation-based active disturbance rejection control is employed for an electro-hydraulic load simulator employing the theory of singular perturbation. In [24], an iterative learning control of the proportional derivative (PD) type in parallel with a traditional PD feedback controller is designed for an electric dynamic load simulator and adaptive learning gains is utilized to repress random measurement noises and periodic disturbances. In [25], an adaptive backstepping controller with a clustering-based fuzzy learning method is presented for the PTS against extra torque, friction, and parametric uncertainties.

Unavoidably, real-world applications are encountered with state constraints. This factor is recognized as a practical limitation that can be dealt with by the barrier Lyapunov function (BLF), as a beneficial solution. This leads to hampering the transgression of constraints by considering *log*-type Lyapunov functions during the stability analysis [26, 27]. Several symmetric and asymmetric BLF-based control schemes have been addressed to guarantee the stability of the overall system subject to the state constraints [28–30].

As a considerable problem in the field of controller theory, choosing the control parameters effects directly on the system performance. Recently, several meta-heuristic algorithms, such as African vultures optimization algorithm (AVOA) [31] or particle swarm optimization (PSO) algorithm [32], were reported for different applications to find optimal values of the control parameters. Moreover, the iterative learning-based algorithm, as a powerful tool in regulating the controller gains, is also received great attention [33]. Therefore, finding the optimal values of the control gains is also studied in this research accordingly.

Inspired by the above observation, this work aims to propose an optimal robust NN learning-based controller for the PTS in the presence of uncertainties subject to the load torque constraint. The design structure is formed by integrating NN with the disturbance observer in the framework of the BLF-based backstepping algorithm while the grey wolf optimization (GWO) algorithm is employed to choose the optimal parameters of the control structure. Thus, the contributions of this article can be highlighted as:

- In the framework of the backstepping method, a new robust NN constrained control scheme is proposed for the PTS subject to the external torque and nonlinear frictions.

- A disturbance observer is integrated with NN to improve the performance of the system while the total estimations are also provided.

- In order to find the optimal values of the controller parameters, the grey wolf optimizer is adopted during the process.

- The proposed idea confirms that the signals are bounded and the tracking error remains in the prespecified bound during the process.

The rest of the article is structured as follows. Section 2 consists of two subsections: the dynamic equations and the NN structure. Section 3 presents the proposed control law and the stability proof. Section 4 illustrates the optimization algorithm. Section 5 describes the results of simulations. Finally, section 6 states the conclusion of this paper.

2. Problem formulation

2.1. Modeling

Figure 1 depicts the schematic of PTS. To model the system, the voltage and current equations of the actuator and torque motor are used and the torque eventuating from nonlinear friction is considered.

The actuator structure is also exhibited on the right side of Figure 1. The voltage and current formulas related to the actuator are expressed by (1) and (2).

$$\mathfrak{L}_a \frac{di_a}{dt} + \mathfrak{R}_a i_a + \mathcal{C}_b \omega_a = u_a \tag{1}$$

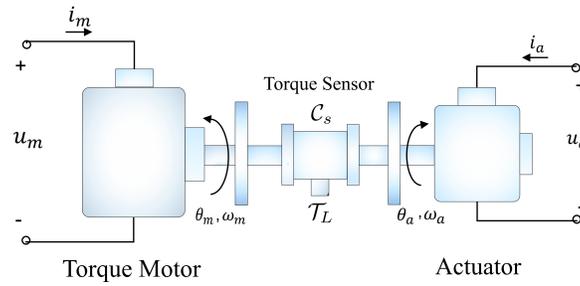$$J_a \frac{d\omega_a}{dt} + B_a \omega_a + \mathfrak{T}_f + \mathfrak{T}_L = \mathfrak{T}_{e_a} \quad , \quad \mathfrak{T}_{e_a} = \mathcal{C}_t i_a \tag{2}$$

Figure 1. The passive torque simulator.

In the above equations, $J_a \left(Nm.s^2/rad \right)$ denotes the actuator rotational inertia, $i_a \left(A \right)$ is the actuator current, $\mathfrak{R}_a \left(\Omega \right)$ denotes the actuator resistance, $\mathfrak{L}_a \left(H \right)$ stands for the actuator inductance, $\mathcal{C}_b \left(V.s/rad \right)$ represents the back electromotive force (back-emf) constant, the actuator rotational speed is described by $\omega_a \left(rad/s \right)$; $u_a \left(V \right)$ denotes the actuator input voltage, the actuator viscous coefficient is written by $B_a \left(Nm.s/rad \right)$ and $\mathcal{C}_t \left(Nm/A \right)$ stands for the torque constant. The actuator electromagnetic torque, the load torque, and the torque derived from the nonlinear friction are represented by $\mathfrak{T}_{e_a} \left(Nm \right)$, $\mathfrak{T}_L \left(Nm \right)$ and $\mathfrak{T}_f \left(Nm \right)$, respectively. The left side of Figure 1 displays the structure of the torque motor. The equations of voltage and current of the torque motor are formulated as:

$$\mathfrak{L}_m \frac{di_m}{dt} + \mathfrak{R}_m i_m + \mathcal{C}_b \omega_m = u_m \tag{3}$$

$$J_m \frac{d\omega_m}{dt} + B_m \omega_m + \mathfrak{T}_f + \mathfrak{T}_L = \mathfrak{T}_{e_m} \quad , \quad \mathfrak{T}_{e_m} = \mathcal{C}_t i_m \tag{4}$$

where J_m $(Nm.s^2/rad)$ denotes the torque motor rotational inertia, i_m (A) is the torque motor current, $\mathfrak{R}_m$ (Ω) denotes the torque motor resistance, $\mathfrak{L}_m$ (H) stands for the torque motor inductance, the torque motor rotational speed is described by ω_m (rad/s); u_m (V) denotes the torque motor input voltage and the torque motor viscous coefficient is written by B_m $(Nm.s/rad)$. The motor electromagnetic torque are represented by $\mathfrak{T}_{e_m}$ (Nm).

The PTS consists of a torque motor, actuator, and torque sensor which is observed in Figure 1. The motor and the actuators are connected using a shaft to transfer torque to each other. Compared to the entire system, the coefficients of inertia and damping related to the torque sensor are negligible. The load torque is expressed as:

$$\mathcal{C}_s(\theta_m - \theta_a) = \mathfrak{T}_L \tag{5}$$

in such a way that $\mathcal{C}_s$ (Nm/rad) is the stiffness of the torque sensor. The angular displacement of the actuator is represented by θ_a (rad). The angular displacement of the torque motor is also described by θ_m (rad).

The torque motor is in a control loop and the load torque $(\mathfrak{T}_L)$ is set by it on the reference torque $(\mathfrak{T}_r)$. Assuming the reference torque $(\mathfrak{T}_r)$ and the input voltage (u_m) are zero, the extra electromagnetic torque $(\mathfrak{T}_{e_m}^*)$ is extracted. Using $\mathfrak{T}_r = 0$ and $u_m = 0$ in (3) and (4) yields:

$$\mathfrak{L}_m \frac{di_m^*}{dt} + \mathfrak{R}_m i_m^* + \mathcal{C}_b \omega_m^* = 0 \tag{6}$$

$$J_m \frac{d\omega_m^*}{dt} + B_m \omega_m^* + \mathfrak{T}_f^* + \mathfrak{T}_L^* = \mathfrak{T}_{e_m}^* \tag{7}$$

where i_m^* (A) and ω_m^* (rad/s) are the torque motor current and torque motor rotational speed in the condition that $\mathfrak{T}_r$ and u_m are zero; the load torque and the torque derived from the nonlinear friction are represented by $\mathfrak{T}_L^*$ (Nm) and $\mathfrak{T}_f^*$ (Nm) when $\mathfrak{T}_r$ and u_m are zero. Diminishing (6) from (3) gives:

$$(i_m - i_m^*)\mathfrak{R}_m + \mathfrak{L}_m \frac{d(i_m - i_m^*)}{dt} + \mathcal{C}_b(\omega_m - \omega_m^*) = u_m \tag{8}$$

Considering $\frac{d\omega_m^*}{dt} = \ddot{\theta}_m^*$, $\frac{d\omega_m}{dt} = \ddot{\theta}_m$, $\omega_m^* = \dot{\theta}_m^*$, and $\omega_m = \dot{\theta}_m$, it is gained by subtracting (7) from (4):

$$J_m(\ddot{\theta}_m - \ddot{\theta}_m^*) + B_m(\dot{\theta}_m - \dot{\theta}_m^*) + \mathfrak{T}_f - \mathfrak{T}_f^* + \mathfrak{T}_L - \mathfrak{T}_L^* = \mathfrak{T}_{e_m} - \mathfrak{T}_{e_m}^* \tag{9}$$

Assuming that after establishing control $\mathfrak{T}_L$ equals $\mathfrak{T}_r$, in the conditions $\mathfrak{T}_r = 0$ we have $\mathfrak{T}_L^* \approx 0$, and by placing in (5) we have $\theta_a = \theta_m^*$, and yields:

$$J_m(\ddot{\theta}_m - \ddot{\theta}_a) + B_m(\dot{\theta}_m - \dot{\theta}_a) + \mathfrak{T}_f - \mathfrak{T}_f^* + \mathfrak{T}_L - \mathfrak{T}_L^* = \mathfrak{T}_{e_m} - \mathfrak{T}_{e_m}^* \tag{10}$$

$$J_m(\ddot{\theta}_m - \ddot{\theta}_a) = (\mathfrak{T}_{e_m} - \mathfrak{T}_{e_m}^*) - B_m(\dot{\theta}_m - \dot{\theta}_a) - \mathfrak{T}_f + \mathfrak{T}_f^* - \mathfrak{T}_L + \mathfrak{T}_L^* \tag{11}$$

$$(\ddot{\theta}_m - \ddot{\theta}_a) = \frac{(\mathfrak{T}_{e_m} - \mathfrak{T}_{e_m}^*)}{J_m} - \frac{B_m}{J_m}(\dot{\theta}_m - \dot{\theta}_a) - \frac{1}{J_m}(\mathfrak{T}_f - \mathfrak{T}_f^* + \mathfrak{T}_L - \mathfrak{T}_L^*) \tag{12}$$

By Multiplying $\mathcal{C}_s$ on each side of the (12), we have:

$$\mathcal{C}_s(\ddot{\theta}_m - \ddot{\theta}_a) = \mathcal{C}_s\frac{(\mathfrak{T}_{e_m} - \mathfrak{T}_{e_m}^*)}{J_m} - \mathcal{C}_s\frac{B_m}{J_m}(\dot{\theta}_m - \dot{\theta}_a) - \frac{\mathcal{C}_s}{J_m}(\mathfrak{T}_f - \mathfrak{T}_f^* + \mathfrak{T}_L - \mathfrak{T}_L^*) \tag{13}$$

Based on (5) and (13), one can write:

$$\ddot{\mathfrak{T}}_L = \mathcal{C}_s\frac{(\mathfrak{T}_{e_m} - \mathfrak{T}_{e_m}^*)}{J_m} - \frac{B_m}{J_m}\dot{\mathfrak{T}}_L - \frac{\mathcal{C}_s}{J_m}(\mathfrak{T}_f - \mathfrak{T}_f^* + \mathfrak{T}_L - \mathfrak{T}_L^*) \tag{14}$$

Substituting $\mathfrak{T}_{e_m} - \mathfrak{T}_{e_m}^* = \mathcal{C}_t(i_m - i_m^*)$ (obtained from (4)) into (14) yields:

$$\ddot{\mathfrak{T}}_L = \frac{\mathcal{C}_s\mathcal{C}_t(i_m - i_m^*)}{J_m} - \frac{B_m}{J_m}\dot{\mathfrak{T}}_L - \frac{\mathcal{C}_s}{J_m}(\mathfrak{T}_f - \mathfrak{T}_f^* + \mathfrak{T}_L - \mathfrak{T}_L^*) \tag{15}$$

On the other hand, the electrical dynamics of the torque motor are faster in comparison with the mechanical dynamics. Hence, $\mathfrak{L}_m\frac{d(i_m - i_m^*)}{dt}$ can be neglected in (8):

$$(i_m - i_m^*) = \frac{u_m}{\mathfrak{R}_m} - \frac{\mathcal{C}_b}{\mathfrak{R}_m}(\omega_m - \omega_a) \tag{16}$$

Substituting (16) into (15) results in:

$$\ddot{\mathfrak{T}}_L = \frac{\mathcal{C}_s\mathcal{C}_t}{J_m}\left(\frac{u_m}{\mathfrak{R}_m} - \frac{\mathcal{C}_b}{\mathfrak{R}_m}(\omega_m - \omega_a)\right) - \frac{B_m}{J_m}\dot{\mathfrak{T}}_L - \frac{\mathcal{C}_s}{J_m}(\mathfrak{T}_f - \mathfrak{T}_f^* + \mathfrak{T}_L - \mathfrak{T}_L^*) \tag{17}$$

$$\ddot{\mathfrak{T}}_L = \frac{\mathcal{C}_s\mathcal{C}_t}{J_m}\frac{u_m}{\mathfrak{R}_m} - \frac{\mathcal{C}_s\mathcal{C}_t}{J_m}\frac{\mathcal{C}_b}{\mathfrak{R}_m}(\omega_m - \omega_a) - \frac{B_m}{J_m}\dot{\mathfrak{T}}_L - \frac{\mathcal{C}_s}{J_m}(\mathfrak{T}_f - \mathfrak{T}_f^* + \mathfrak{T}_L - \mathfrak{T}_L^*) \tag{18}$$

Employing the first-order derivative of (5) in (18) gives the following result:

$$\ddot{\mathfrak{T}}_L = \frac{\mathcal{C}_s\mathcal{C}_t}{J_m}\frac{u_m}{\mathfrak{R}_m} - \frac{\mathcal{C}_t}{J_m}\frac{\mathcal{C}_b}{\mathfrak{R}_m}\dot{\mathfrak{T}}_L - \frac{B_m}{J_m}\dot{\mathfrak{T}}_L - \frac{\mathcal{C}_s}{J_m}(\mathfrak{T}_f - \mathfrak{T}_f^* + \mathfrak{T}_L - \mathfrak{T}_L^*) \tag{19}$$

It can be rewritten as:

$$\ddot{\mathfrak{T}}_L = \frac{\mathcal{C}_s\mathcal{C}_t}{J_m\mathfrak{R}_m}u_m - \left(\frac{\mathcal{C}_t\mathcal{C}_b}{J_m\mathfrak{R}_m} + \frac{B_m}{J_m}\right)\dot{\mathfrak{T}}_L - \frac{\mathcal{C}_s}{J_m}\mathfrak{T}_L - \frac{\mathcal{C}_s}{J_m}(\mathfrak{T}_f - \mathfrak{T}_f^* - \mathfrak{T}_L^*) \tag{20}$$

By defining f and placing $\mathfrak{T}_L^*$ from (7) we have:

$$f = \frac{\mathcal{C}_s}{J_m}(\mathfrak{T}_f - \mathfrak{T}_f^* - \mathfrak{T}_L^*) = \frac{\mathcal{C}_s}{J_m}(\mathfrak{T}_f - \mathfrak{T}_{e_m}^* + J_m\ddot{\theta}_a + B_m\dot{\theta}_a) \tag{21}$$

To compute and simulate the nonlinear friction effect on torque, we employ the LuGre model. It explains the behavior of the dynamic frictions such as viscous friction and Stribeck effect, variable static force, and presliding displacement simultaneously [34]. Based on the LuGre model, the nonlinear friction effect on the torque can be modeled through the following equations:

$$\mathfrak{T}_f = \sigma_0 z + \sigma_1 \dot{z} + \sigma_2 v \tag{22}$$

in which

$$\dot{z} = v - \frac{\sigma_0 \, |v|}{\mathfrak{g}(v)} z \tag{23}$$

$$\mathfrak{g}(v) = \mathfrak{F}_c + (\mathfrak{F}_c - \mathfrak{F}_s)e^{-\left(\frac{v}{v_s}\right)^2} \tag{24}$$

Based on the above explanations, σ_2 is the viscous friction coefficient, σ_1 denotes the damping term, σ_0 is the stiffness of the bristles, $\mathfrak{g}(v)$ represents the Stribeck effect, z is the average briste defection, v_s is the stribeck velocity, $\mathfrak{F}_s$ stands for the static friction, and $\mathfrak{F}_c$ describes the coulomb friction. The LuGre model parameters are given in Table 1 [35].

Table 1. The parameters of LuGre model.

Parameter	Value	Unit
σ_0	10^5	N/m
σ_1	$\sqrt{10^5}$	Ns/m
σ_2	0.4	Ns/m
$\mathfrak{F}_c$	1	N
$\mathfrak{F}_s$	1.5	N
v_s	0.001	m/s

Therefore, the below formula related to the output torque can be obtained as:

$$\ddot{\mathfrak{T}}_L = -a\dot{\mathfrak{T}}_L + bu_m - c\mathfrak{T}_L - f \tag{25}$$

where $a = \frac{\mathcal{C}_t \mathcal{C}_b}{J_m \mathfrak{R}_m} + \frac{B_m}{J_m}$, $b = \frac{\mathcal{C}_s \mathcal{C}_t}{J_m \mathfrak{R}_m}$ and $c = \frac{\mathcal{C}_s}{J_m}$.

2.2. Neural network structure

Radial basis function networks (RBFNs) are recognized as a kind of artificial neural network adopted for various tasks. The universal approximation and the fast learning speed are the key points for RBFN, distinct from other NNs [36, 37]. As shown in Figure 2, the RBFN consists of the input layer, the hidden layer, and the output layer. The activation function used in the hidden layer is determined by the distance of each input data from the established centers and is utilized to approximate the output based on the input values as shown in (26):

$$\hat{Q} = \hat{\Gamma}_1^T \phi = \sum_{i=1}^{n} \sum_{j=1}^{m} W_i \cdot \phi_i(\|x_i - c_j\|) \tag{26}$$

in which $\hat{\Gamma}_1$ is the estimated weight vector, ϕ is the nonlinear function of the inputs, n is the data number, m denotes the number of neurons, $x_i = (x_1, ..., x_n) \in R^n$ represents the input data, $c_j = (c_1, ..., c_m) \in R^m$ is the center of neurons, $\phi_i = (\phi_1, ..., \phi_n) \in R^n$ stands for the activation function and $W_i = (W_1, ..., W_n) \in R^n$ denotes the neuron weights.
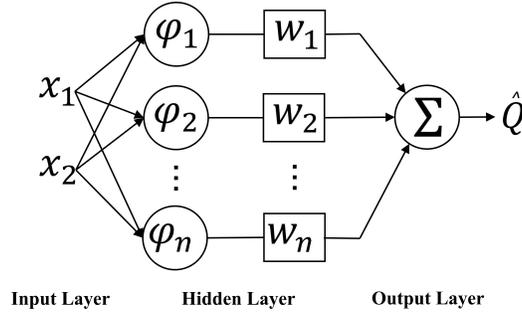
Figure 2. Structure of the RBFN

The Gaussian function is used to create the activation function as:

$$\phi_i(\|x_i - c_j\|) = exp\left(-\frac{(\|x_i - c_j\|)^2}{2\sigma^2}\right) \tag{27}$$

where σ describes the Gaussian function variance, which defines the degree of dispersion of the data. It should be mentioned that in this paper, f_1 is an unknown term, described by the structure of RBFN as $f_1 = \Gamma_1^{*T}\phi + \epsilon_1$ in which Γ_1^* is the optimal weight vector such that $sup\left|f_1 - \Gamma_1^{*T}\phi\right| \leq \epsilon_1$ for any $|\epsilon_1| < \epsilon_m$ [39]. On the other hand, since the optimal weight vector is not available, the estimated weight vector $\hat{\Gamma}_1$ should be obtained by the adaptive law derived from the Lyapunov-based stability analysis. More details are given in the next section.

3. Control design algorithm and stability analysis

In this part, a robust adaptive BLF-based NN learning controller using a disturbance observer is proposed for the PTS. By defining $\mathfrak{T}_L = x_1$ and $\dot{\mathfrak{T}}_L = x_2$, the system dynamics (25) subject to the external disturbance $d(t)$ can be expressed as:

$$\dot{x}_1 = x_2 \tag{28}$$

$$\dot{x}_2 = f_1 - bu + d(t)$$

where $f_1 = -ax_2 - cx_1 + f$. The purpose of control design is to realize good tracking performance in such a way that the output stays within $|x_1| \leq k_c$. It is worth pointing out that the following assumptions and lemma are employed in the stability analysis.

Assumption 1: The desired path $x_1^d(t)$ and its time-derivatives up to the required order satisfy $|x_1^d(t)| \leq A_0 < k_c$ and $|x_1^{d(j)}(t)| \leq A_j$ in such a way that k_c and A_j are positive constants.

Assumption 2 [38]: The total disturbance D_1, including the time-varying external disturbance $d(t)$ and the error of NN approximation ϵ_1, can satisfy $|D_1| \leq \varrho_1$ and $\left|\dot{D}_1\right| \leq \zeta_1$ where ϱ_1 and ζ_1 are unknown positive constants.

Lemma 1 [39]: For any positive constant k_a, the following inequality holds for the interval $|\omega_1| < |k_a|$:

$$\log\frac{k_a^2}{k_a^2 - \omega_1^2} \leq \frac{\omega_1^2}{k_a^2 - \omega_1^2} \tag{29}$$

Based on the backstepping algorithm [40], two steps are provided for designing the proposed controller as follows:

Step 1)

The tracking error is described as:

$$\omega_1 = x_1 - x_1^d \tag{30}$$

Choose virtual control as:

$$\beta_1 = -k_1\omega_1 + \dot{x}_1^d \tag{31}$$

in which $k_1 > 0$. The derivative of ω_1 is obtained as:

$$\dot{\omega}_1 = \dot{x}_1 - \dot{x}_1^d = x_2 - \dot{x}_1^d = \omega_2 + \beta_1 - \dot{x}_1^d \tag{32}$$

Thus,

$$\dot{\omega}_1 = -k_1\omega_1 + \omega_2 \tag{33}$$

Considering $|\omega_1| < k_a$, we choose the Lyapunov function as:

$$V_1 = 0.5 \log(\frac{k_a^2}{k_a^2 - \omega_1^2}) \tag{34}$$

Using (32), the derivative of V_1 is obtained as:

$$\dot{V}_1 = \frac{\omega_1(\omega_2 + \beta_1 - \dot{x}_1^d)}{k_a^2 - \omega_1^2} \tag{35}$$

Employing (33) in (35) gives the following result:

$$\dot{V}_1 = \frac{-k_1\omega_1^2}{k_a^2 - \omega_1^2} + \frac{\omega_1\omega_2}{k_a^2 - \omega_1^2} \tag{36}$$

Step 2)

The derivative of tracking error for the second subsystem is expressed as:

$$\dot{\omega}_2 = \dot{x}_2 - \dot{\beta}_1 = \Gamma_1^{*T}\phi + \epsilon_1 + d(t) - bu - \dot{\beta}_1 = \Gamma_1^{*T}\phi + D_1 - bu - \dot{\beta}_1 \tag{37}$$

where $D_1 = d(t) + \epsilon_1$. The Lyapunov function is considered as:

$$V_2 = V_1 + \frac{1}{2}\omega_2^2 + \frac{1}{2}\tilde{\Gamma}_1^T\gamma_1^{-1}\tilde{\Gamma}_1 + \frac{1}{2}\tilde{D}_1^2 \tag{38}$$

where $\gamma_1 > 0$. Also, $\tilde{\Gamma}_1$ and $\tilde{D}_1$ are considered as $\Gamma_1^{*T} - \hat{\Gamma}_1$ and $D_1 - \hat{D}_1$, respectively. Note that $\hat{\Gamma}_1$ is the estimated NN weight vector and $\hat{D}_1$ is the disturbance observer, defined later. The derivative of V_2 can be

expressed as:

$$\dot{V}_2 = \frac{-k_1\omega_1^2}{k_a^2 - \omega_1^2} + \omega_2\left(\Gamma_1^{*T}\phi + D_1 - bu - \dot{\beta}_1 + \frac{\omega_1}{k_a^2 - \omega_1^2}\right) - \tilde{\Gamma}_1^T\gamma_1^{-1}\dot{\hat{\Gamma}}_1 + \tilde{D}_1(\dot{D}_1 - \dot{\hat{D}}_1) \tag{39}$$

The control law is suggested as:

$$u = \frac{-\hat{\Gamma}_1^T\phi - k_2\omega_2 - \frac{\omega_1}{k_a^2 - \omega_1^2} + \dot{\beta}_1 - \hat{D}_1}{-b} \tag{40}$$

in which $k_2 > 0$. Hence,

$$\dot{V}_2 = \frac{-k_1\omega_1^2}{k_a^2 - \omega_1^2} + \omega_2(-k_2\omega_2 + \tilde{\Gamma}_1^T\phi + \tilde{D}_1) - \tilde{\Gamma}_1^T\gamma_1^{-1}\dot{\hat{\Gamma}}_1 + \tilde{D}_1(\dot{D}_1 - \dot{\hat{D}}_1) \tag{41}$$

However, the disturbance observer can be described as:

$$\hat{D}_1 = L_1\left(x_2 - \chi_2\right) \tag{42}$$

$$\dot{\chi}_2 = \hat{\Gamma}_1^T\phi - bu + \hat{D}_1 - L_1^{-1}\omega_2$$

where $L_1 > 0$ and χ_2 is an auxiliary variable. The derivative of (42) is obtained as:

$$\dot{\hat{D}}_1 = L_1\left(\dot{x}_2 - \dot{\chi}_2\right) = L_1\left(\tilde{\Gamma}_1^T\phi + \tilde{D}_1\right) + \omega_2 \tag{43}$$

Using (43) in (41), we have:

$$\dot{V}_2 = \frac{-k_1\omega_1^2}{k_a^2 - \omega_1^2} - k_2\omega_2^2 + \tilde{\Gamma}_1^T\left(\omega_2\phi - \gamma_1^{-1}\dot{\hat{\Gamma}}_1\right) + \tilde{D}_1\left(\dot{D}_1 - L_1\left(\tilde{\Gamma}_1^T\phi + \tilde{D}_1\right)\right) \tag{44}$$

The adaptive law is chosen as:

$$\dot{\hat{\Gamma}}_1 = \gamma_1\left(\omega_2\phi - \delta_1\hat{\Gamma}_1\right) \tag{45}$$

where $\delta_1 > 0$. Employing Young inequality [41], we have:

$$\tilde{D}_1\dot{D}_1 \leq \frac{1}{2}\tilde{D}_1^2 + \frac{1}{2}\zeta_1^2 \tag{46}$$

$$-\tilde{D}_1\tilde{\Gamma}_1^T\phi \leq \frac{1}{2}\rho_1\tilde{D}_1^2\eta_1^2 + \frac{1}{2\rho_1}\tilde{\Gamma}_1^T\tilde{\Gamma}_1$$

$$\tilde{\Gamma}_1^T\hat{\Gamma}_1 \leq -\frac{1}{2}\tilde{\Gamma}_1^T\tilde{\Gamma}_1 + \frac{1}{2}\|\Gamma_1^*\|^2$$

in which η_1 and ρ_1 are positive constants. Using (45) and (46) in (44), $\dot{V}_2$ is obtained as:

$$\dot{V}_2 \leq \frac{-k_1\omega_1^2}{k_a^2 - \omega_1^2} - k_2\omega_2^2 - \left(\frac{\delta_1}{2} - \frac{L_1}{2\rho_1}\right)\tilde{\Gamma}_1^T\tilde{\Gamma}_1 - \left(L_1 - \frac{L_1\rho_1}{2}\eta_1^2 - \frac{1}{2}\right)\tilde{D}_1^2 + \left(\frac{\delta_1}{2}\|\Gamma_1^*\|^2 + \frac{1}{2}\zeta_1^2\right) \tag{47}$$

Thus, one can write:

$$\dot{V}_2 \leq -AV_2 + B \tag{48}$$

where
$A = \min\left\{2k_1, 2k_2, \gamma_1\left(\delta_1 - \frac{L_1}{\rho_1}\right), (2L_1 - L_1\rho_1\eta_1^2 - 1)\right\}$ and $B = \{\frac{\delta_1}{2}\|\Gamma_1^*\|^2 + \frac{1}{2}\zeta_1^2\}$. Thus, the uniformly ultimate boundedness (UUB) stability of the closed-loop system is realized. According to the Assumption 1 and the boundedness of ω_1, it is inferred that $|x_1| < k_a + A_0 \leq k_c$. The block diagram of the proposed framework is also exhibited in Figure 3.
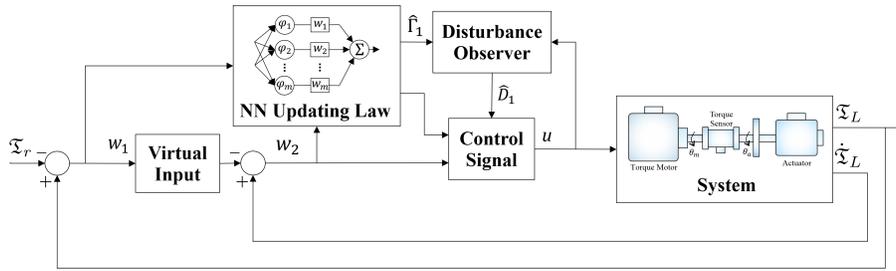

Figure 3. The block diagram of the proposed framework.

4. Grey wolf optimizer

Grey wolf optimizer, as a meta-heuristic optimization algorithm, implements the mathematical model of the leadership hierarchy and hunting mechanism of grey wolves in nature. The search procedure begins with considering a random population of grey wolves. The possible position of the prey is estimated by tuning the search agents, including the number of iterations, beta, delta and alpha parameters. Each factor leads to updating the distance of the wolf from the prey [42, 43].

The distance between the wolves and the prey is explained as follows:

$$\vec{G} = |\vec{C} \cdot \vec{X}_P(t) - \vec{X}(t)| \tag{49}$$

$$\vec{X}(t+1) = \vec{X}_P(t) - \vec{A} \cdot \vec{G} \tag{50}$$

in which $\vec{X}$ denotes the position vector of a grey wolf, $\vec{X}_P$ represents the position vector of the prey, and t indicates the current iteration. $\vec{A}$ and $\vec{C}$ are coefficient vectors that are computed as:

$$\vec{A} = 2\vec{a} \cdot \vec{r}_1 - \bar{a} \tag{51}$$

$$\vec{C} = 2 \cdot \vec{r}_2 \tag{52}$$

in which $\vec{r}_1$ and $\vec{r}_2$ are random vectors in $[0,1]$ that allow wolves to reach any position around the prey, and $\vec{a}$ is employed to express approaching the prey that is linearly reduced from 2 to 0 during the optimization

process. Using the error dynamics ω_1 and ω_2, the cost function is also expressed as follows:

$$F = \int_0^t |\omega_1 + \omega_2| dt \tag{53}$$

where t is the run time. As shown in Figure 4, the flowchart presents the performance of the GWO.
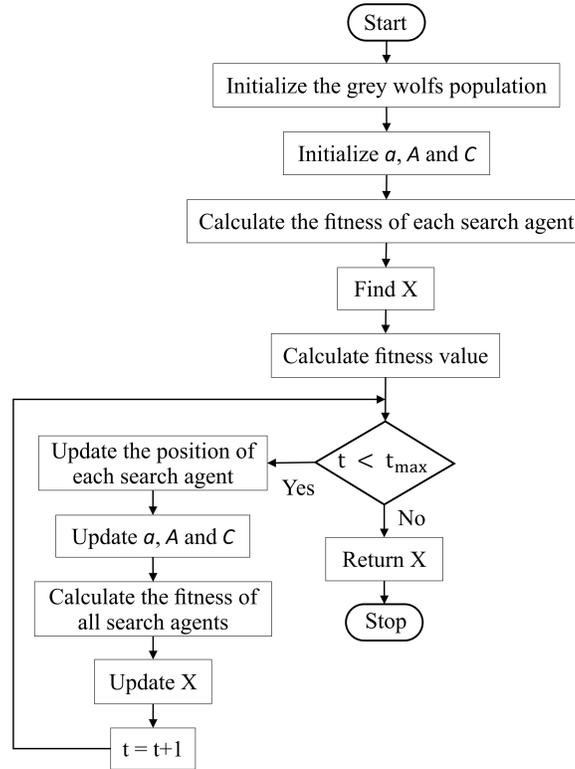

Figure 4. Flowchart of the GWO.

Remark 1: Increasing controller parameters k_1 and k_2 leads to achieving the small value for the tracking error. However, large values of the aforementioned coefficients lead to growing the control input which may violate the predefined bounds. Furthermore, increasing γ_1 and L_1 leads to improving the estimation task of the control system.

Remark 2: Different from the relevant works on the PTS, our presented controller illustrates the following properties:

1) In contrast with [45] and [46], better tracking performance is realized by deriving a new backstepping-based robust learning control law instead of the conventional backstepping method.

2) Integrating NN with disturbance observer leads to improving the estimation purpose, which has not been studied in [15, 47].

3) According to our knowledge, proposing a BLF-based learning controller for PTS has not been discussed before.

Remark 3: To show the efficacy of the current work in comparison with the given controller in [25], the following points are highlighted:

1) To enhance the robust behavior of the proposed controller, an NN-based disturbance observer is designed in this study while it has not been addressed in [25].

2) The issue of output constraint is tackled by employing the BLF technique while it has not been studied in [25].

3) Compared with [25], in which the control parameters were chosen by the trial and error technique, the design parameters of this study are optimally tuned by adopting the GWO algorithm.

Remark 4: Apart from the reported advantages of the proposed controller (see Remarks 2 and 3), we can also add the challenges of the proposed control scheme, which can be considered as future work. In the current work, the constraint bound has been considered as constant values. In order to bring the proposed control framework closer to real-world applications, the constraint bound needs to be considered as the time-varying values. Besides, although the NN structure is a powerful approximator, this algorithm may increase the computational burden. Thus, using the function approximation technique (FAT) can cope with this problem [44]. This issue can be also studied in our future work.

Remark 5: Compared with [48], the tracking error of the proposed controller has remained within a narrower bound. This is due to proposing a disturbance observer-based BLF control scheme, which has not been used in our previous research. (It is worth noting that the predefined bound in the current work is set to 0.005 while it was chosen as 0.01 in the previous research). In addition, by comparing the control signals of both control approaches, it can be inferred that better tracking responses have been achieved by injecting less control effort.

Remark 6: The employed disturbance observer has a nonlinear structure due to the existence of term $\hat{\Gamma}_1^T \phi$ in which ϕ is the regressor matrix constructed by nonlinear activation functions derived from RBFNs. Furthermore, it can be considered as an extension of the disturbance observer given by [49] since both approaches need an auxiliary state, denoted by χ_2 in (42), obtained from an adaptation mechanism. However, the current disturbance observer is based on a model-free approach while the mentioned disturbance observer has a model-based structure. The stability of the current disturbance observer has been proven along with the stability proof of the proposed controller in a compact form. This leads to achieving UUB stability. On the other hand, as given by (46), utilizing the Young inequality remains constant terms as $\frac{\delta_1}{2}\|\Gamma_1^*\|^2$ and $\frac{1}{2}\zeta_1^2$, which prevent the exponential stability in our proof. It is worth noting that the UUB stability is a well-known stability criterion in the field of backstepping-based designs, as clearly found in the related literature [26], [38], [44].

5. Simulation results

As presented before, the first section is dedicated to the model description, which leads to obtaining the output torque equation as mentioned in (25), and also neural network (NN) structure (26). After that, the modeling equation is written in the form of (28), which is used as the system dynamics for the control design and simulations. Besides, f_1 is considered as an unknown term in (28), which is approximated by the NN structure. Thus, inspired by the (26), the approximated term is modeled as $\hat{f}_1 = \hat{\Gamma}_1^T \phi$ in the design procedure. Therefore, using the virtual input (31), the control input (40), the disturbance observer (42), and the adaptive law (45), the results of the simulation are achieved in this part. The system parameters are borrowed from [45], given as $\mathcal{C}_s = 950$, $\mathcal{C}_t = 5.732$, $\mathcal{C}_b = 5.732$, $J_m = 0.04$, $\mathfrak{R}_m = 7.5$, $B_m = 0.244$. The initial conditions are set to zero for the state variables x_1 and x_2. The input signals for the neural network structure are the state variables x_1

and x_2, as defined by (28). Three centers c_j, are evenly spaced in $[-1, 1] \times [-1, 1]$ and the variance is set to 2 to form the activation function. Note that the RBFN weight $\hat{\Gamma}_1$ is updated by the adaptive law, given by (45). The control parameters are tuned by the GWO algorithm as $k_1 = 2.887$, $k_2 = 3.490$, $\gamma_1 = 11.218$, $\delta_1 = 0.115$, and $L_1 = 4.255$. Figure 5 presents the best optimal value of the defined cost function found by GWO. In order to test the capability of the disturbance observer utilized in the proposed controller design, white noise with a variance of 0.1 is considered during the operation.

The results of the control system are presented in the first subsection, and then, a comparison scenario with a relevant method [45] is given in the second subsection.
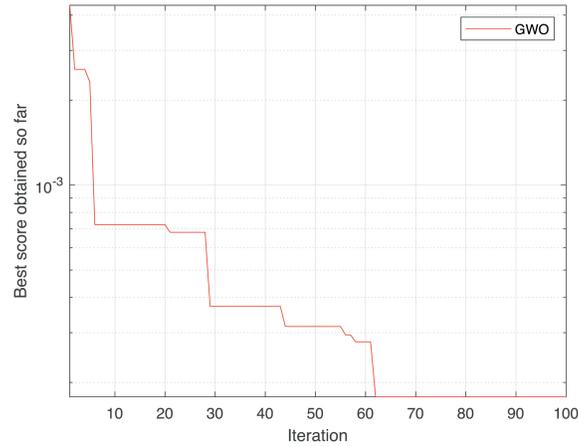

Figure 5. The best optimal value of the defined cost function.

5.1. The results related to the proposed control law

To achieve the proper performance in tracking the desired torque, estimation of the uncertainties caused by additional torque, nonlinear friction, and parameter uncertainties along with the estimation of the disturbances applied to the system, plays an important role.

Following this point, the disturbance observer-based neural network learning method is employed to estimate the uncertainties. By adding a neural network learning structure and disturbance observer to the BLF-based backstepping design, the control law is formed to inject into the PTS for tracking the desired torque. Thus, the results are recorded in Figures 8-12. The result of total uncertainty estimation including extra torque, external disturbance, and the torque due to nonlinear friction is shown in Figure 6.

The torque tracking response is exhibited in Figure 7. The difference between the torque resulting from the proposed method and the desired torque is considered as a tracking error (ω_1), which is observed in Figure 8. In addition, the performance of the second error surface (i.e. ω_2) is also given in Figure 8. The well-behaved control signal is represented by Figure 9. From the results given by Figures 8-10, it can be deduced that the suggested control law provides satisfactory performance both for tracking and estimation purposes. Changing the K_a value and its effect on the tracking error are shown in Figure 10. From this figure, it can be found that the tracking error is restricted based on the K_a value, indicating the constraint of the load torque.
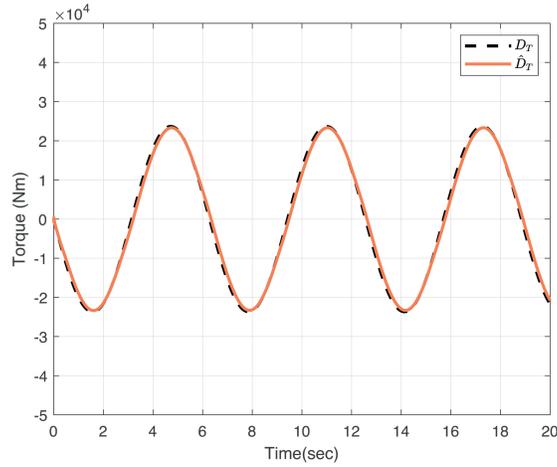
Figure 6. The approximation of total unknown terms.

Remark 7: The total uncertainty is $D_T = f_1 + d(t)$ while the total estimation is $\hat{D}_T = \hat{\Gamma}_1^T \phi + \hat{D}_1$. Since NN and disturbance observer are sharing data, it cannot be precisely determined whether $\hat{\Gamma}_1^T \phi$ can identify f_1. Thus, the goal of the proposed control scheme is gained from the estimation point of view, if the total estimation $\hat{D}_T$ can follow the total uncertainty D_T with high accuracy. As a result, the estimation task is also confirmed by Figure 6.

Remark 8: According to Figure 10, while the predetermined bound becomes narrower, from 0.01 to 0.0025, no violation occurs. This shows the ability of the proposed control law with respect to constraint control.

5.2. Comparison scenario

In this subsection, the performance of the presented control system is compared with the results obtained from a relevant control technique [45]. The tracking performance of both methods is depicted in Figure11. It can be deduced that the tracking error of the proposed method stays within the predefined bound while the result obtained from [45] violates the bound. In other words, our proposed method is successful in realizing the load torque constraint.
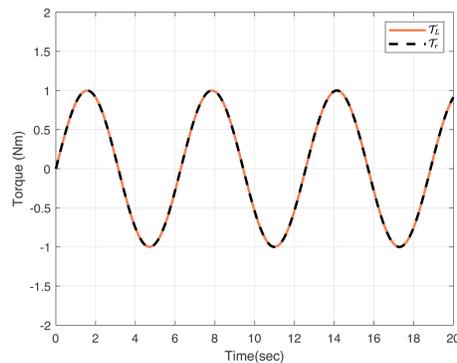

Figure 7. Tracking response by applying the proposed method: $\mathfrak{T}_L$ (solid line), $\mathfrak{T}_r$ (dash line).
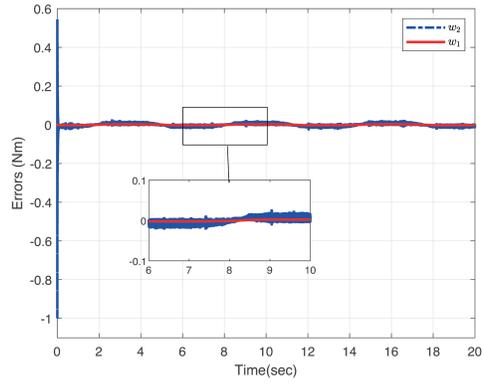
Figure 8. Torque tracking errors after applying the proposed method.
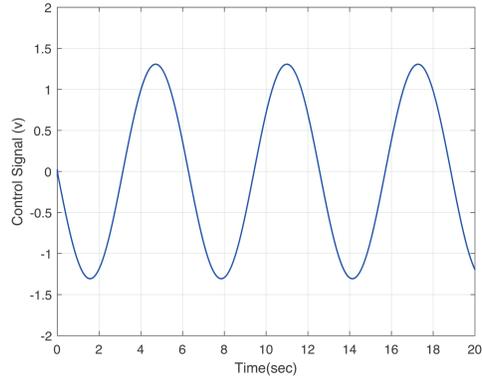

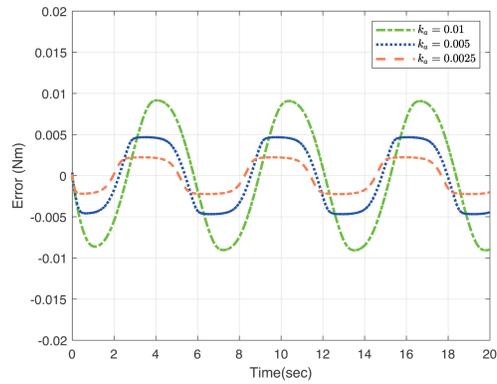**Figure 9**. Control effort.

Figure 10. Comparison of tracking error affected by different values of k_a.
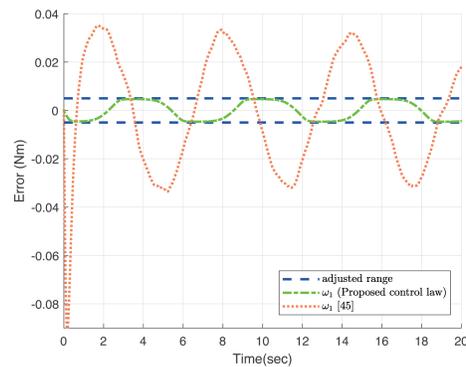
Figure 11. Comparison between the proposed control system and [45] in view of tracking performance.

6. Conclusion

This research presents an adaptive robust constrained control law for passive torque simulators in the presence of parametric uncertainties, nonlinear friction, and extra torque. Besides, an adaptive RBFN shares the information with the designed disturbance observer to approximate total uncertainties. This leads to promoting the robust performance of the system. The boundedness of the signals in the overall system is ensured using the Lyapunov theorem. The supremacy of the proposed control framework to the conventional control methods is also exhibited by the simulations. In the future, we will study the effects of actuator fault and input constraints on the performance of PTS, simultaneously. In addition, we can employ the quadratic program-based safety constraint methodology to upgrade our constraint-based design as a future work [50].

References

[1] Li C, Pan X, Wang G. Torque tracking control of electric load simulator with active motion disturbance and nonlinearity based on T-S fuzzy model. Asian Journal of Control 2020; 22 (3): 1280–1294.

[2] Shamisa A, Kiani Z. Robust fault-tolerant controller design for aerodynamic load simulator. Aerospace Science and Technology 2018; 78: 332–341.

[3] Koh DW, Park SY, Kim DH, Choi KH. Development of a hardware-in-the-loop simulator for spacecraft attitude control using thrusters. Journal of Astronomy and Space Sciences 2009; 26 (1): 47–58.

[4] Jeon SW, Jung S. Hardware-in-the-loop simulation for the reaction control system using PWM-based limit cycle analysis. IEEE Transactions on control systems technology 2011; 20 (2): 538–545.

[5] Li H, Steurer M, Shi K, Woodruff S, Zhang D. Development of a unified design, test, and research platform for wind energy systems based on hardware-in-the-loop real-time simulation. IEEE Transactions on Industrial Electronics 2006; 53 (4): 1144–1151.

[6] Crăciun O, Florescu A, Munteanu I, Bratcu AI, Bacha S et al. Hardware-in-the-loop simulation applied to protection devices testing. International Journal of Electrical Power and Energy Systems 2014; 54: 55–64.

[7] Lee M, Lee H, Lee KS, et al. Development of a hardware in the loop simulation system for electric power steering in vehicles.International journal of Automotive technology 2011; 12 (5): 733.

[8] Palladino A, Fiengo G, Lanzo D. A portable hardware-in-the-loop (HIL) device for automotive diagnostic control systems. *ISA Transactions* 2012; 51 (1): 229–236.

[9] Hwang A, Yoon S, Kim TY, Kwon DY, Choi C et al. Verification of unmanned underwater vehicle with velocity over 10 knots guidance control system based on hardware in the loop simulation. In: IEEE.; 2009: 1–5.

[10] Martin A, Emami MR. Dynamic load emulation in hardware-in-the-loop simulation of robot manipulators. IEEE Transactions on Industrial Electronics 2010; 58 (7): 2980–2987.

[11] Chhabra R, Emami MR. A holistic concurrent design approach to robotics using hardware-in-the-loop simulation. Mechatronics 2013; 23 (3): 335–345.

[12] Burbank JL, Kasch W, Ward J. An introduction to network modeling and simulation for the practicing engineer. John Wiley & Sons . 2011.

[13] Gawthrop P, Virden D, Neild S, Wagg D. Emulator-based control for actuator-based hardware-in-the-loop testing.Control Engineering Practice 2008; 16 (8): 897–908.

[14] Ullah N, Wang SP. Backstepping Control of Electrical Load Simulator with Adaptive Tracking Performance Controller. In: . 245. Trans Tech Publ. ; 2013: 310–315.

[15] Yang B, Liu F, Zhang M. A loading control strategy for electric load simulator based on new mapping approach and fuzzy inference in Cerebellar Model Articulation Controller. Measurement and Control 2019; 52 (1-2): 131–144.

[16] Fu Z, Wang S, Wang X. ESO-based adaptive robust force control of linear electric load simulator. 2018.

[17] Li Z, Shang Y, Jiao Z, Wu S, Yao J. Surplus Torque elimination control of electro-hydraulic load simulator based on actuator velocity input feedforward compensating method. Journal of Dynamic Systems, Measurement, and Control 2018; 140 (10).

[18] Li C, Li Y, Wang G. H_∞ output tracking control of electric-motor-driven aerodynamic load simulator with external active motion disturbance and nonlinearity. Aerospace Science and Technology 2018; 82: 334–349.

[19] Tian W, Pan W, Shao Y, Xu B, Liu H et al. Individual pitch control strategy for reducing aerodynamic loads and torque ripples. IEEJ Transactions on Electrical and Electronic Engineering 2019; 14 (11):1624–1632.

[20] Jing C, Xu H, Jiang J. Dynamic surface disturbance rejection control for electro-hydraulic load simulator. Mechanical Systems and Signal Processing 2019; 134: 106293.

[21] Borges FAP, Perondi EA, Cunha MAB, Sobczyk MR. A neural network-based inversion method of a feedback linearization controller applied to a hydraulic actuator. Journal of the Brazilian Society of Mechanical Sciences and Engineering 2021; 43 (5): 1–19.

[22] Zhang B, Li C, Wang T, Wang Z, Ma H. Design and experimental study of zero-compensation steering gear load simulator with double torsion springs. Measurement 2019; 148: 106930.

[23] Jing C, Xu H, Jiang J. Practical torque tracking control of electro-hydraulic load simulator using singular perturbation theory. ISA Transactions 2020; 102: 304–313.

[24] Dai M, Qi R, Zhao Y, Li Y. PD-Type Iterative Learning Control with Adaptive Learning Gains for High-Performance Load Torque Tracking of Electric Dynamic Load Simulator. Electronics 2021;10 (7): 811.

[25] Saadat SA, Fateh MM, Keighobadi J. Adaptive state augmented clustering-based fuzzy learning control of a passive torque simulator. International Journal of Dynamics and Control 2021: 1–13.

[26] Keighobadi J, Fateh MM, Xu B. Adaptive fuzzy voltage-based backstepping tracking control for uncertain robotic manipulators subject to partial state constraints and input delay. Nonlinear Dynamics 2020; 100 (3): 2609–2634.

[27] Fang Y, Kong H, Ding D. Novel fast terminal sliding mode controller with current constraint for permanent-magnet synchronous motor. Turkish Journal of Electrical Engineering and Computer Sciences 2021; 29 (3): 1821–1835.

[28] Li Y, Liu Z, Wang Z, Yin Y, Zhao B. Adaptive control of teleoperation systems with prescribed tracking performance: a BLF-based approach. International Journal of Control 2022; 95 (6): 1600–1610.

[29] Yang Z, Dong C, Zhang X, Wang G. Full-state time-varying asymmetric constraint control for non-strict feedback nonlinear systems based on dynamic surface method. Scientific Reports 2022; 12 (1): 10469.

[30] Wei Y, Wang H, Tian Y. Asymmetric time-varying BLF-based model-free hybrid force/position control for SEA-based 2-DOF manipulator. International Journal of Adaptive Control and Signal Processing. 2023; 37 (7): 1716–1737.

[31] R.-C. Roman, R.-E. Precup, E. M. Petriu, M. Muntyan. "Fictitious reference iterative tuning of discrete-time model-free control for tower crane systems," *STUDIES IN INFORMATICS AND CONTROL*, vol. 32, no. 1, pp. 5–14, 2023.

[32] Saadat SA, Ghamari SM, Mollaee H. Adaptive backstepping controller design on Buck converter with a novel improved identification method. IET Control Theory & Applications 2022; 16 (5): 485–495.

[33] Chi R, Li H, Shen D, Hou Z, Huang B. "Enhanced p-type control: Indirect adaptive learning from set-point updates," IEEE Transactions on Automatic Control, vol. 68, no. 3, pp. 1600–1613, 2022.

[34] Wang X, Wang S, Yao B. Adaptive robust control of linear electrical loading system with dynamic friction compensation. In: IEEE.; 2010: 908–913.

[35] De Wit CC, Olsson H, Astrom KJ, Lischinsky P. A new model for control of systems with friction. IEEE Transactions on Automatic Control 1995; 40 (3): 419–425.

[36] Broomhead DS, Lowe D. Radial basis functions, multi-variable functional interpolation and adaptive networks. tech. rep., Royal Signals and Radar Establishment Malvern (United Kingdom); 1988.

[37] Awad M. Enhanced hybrid method of divide-and-conquer and RBF neural networks for function approximation of complex problems. Turkish Journal of Electrical Engineering and Computer Sciences 2017; 25 (2): 1095–1105.

[38] Xu B, Sun F. Composite intelligent learning control of strict-feedback systems with disturbance. *IEEE Transactions on Cybernetics* 2018; 48 (2): 730–741.

[39] Ren B, Ge SS, Tee KP, Lee TH. Adaptive neural control for output feedback nonlinear systems using a barrier Lyapunov function. IEEE Transactions on Neural Networks 2010; 21 (8): 1339–1345.

[40] Keighobadi J, Fateh MM. Adaptive Robust Tracking Control Based on Backstepping Method for Uncertain Robotic Manipulators Including Motor Dynamics. International Journal of Industrial Electronics Control and Optimization 2021; 4 (1): 13–22.

[41] Deng H, Krstić M. Stochastic nonlinear stabilization—I: A backstepping design. Systems & Control Letters 1997; 32 (3): 143–150.

[42] Mirjalili S, Mirjalili SM, Lewis A. Grey wolf optimizer. Advances in Engineering Software 2014; 69: 46–61.

[43] Majeed MM, Patri SR. An enhanced grey wolf optimization algorithm with improved exploration ability for analog circuit design automation. Turkish Journal of Electrical Engineering and Computer Sciences 2018;26 (5): 2605–2617.

[44] Keighobadi J, Xu B, Alfi A, Arabkoohsar A, Nazmara G. Compound FAT-based prespecified performance learning control of robotic manipulators with actuator dynamics. ISA Transactions 2022; 131: 246–263.

[45] Ullah N, Wang S, Wang X. Fuzzy backstepping torque control of passive torque simulator with algebraic parameters adaptation. Journal of Electrical Engineering 2015; 66 (4): 203–213.

[46] Ullah N, Aziz-Al Ahmadi A. Non integer order modeling and control of aerodynamic load simulator system. IEEE Access 2019; 7: 160177–160190.

[47] Xingjian W, Shaoping W, Pan Z. Adaptive fuzzy torque control of passive torque servo systems based on small gain theorem and input-to-state stability. Chinese Journal of Aeronautics 2012; 25 (6): 906–916.

[48] Saadat SA, Fateh MM, Keighobadi J. Backstepping-based adaptive constrained control of passive torque simulator using function approximation technique. in 2022 30th International Conference on Electrical Engineering (ICEE). IEEE, 2022, pp.603–608.

[49] Chen WH, Ballance DJ, Gawthrop PJ, O'Reilly J. A nonlinear disturbance observer for robotic manipulators. IEEE Transactions on Industrial Electronics 2000; 47 (4): 932-938.

[50] Ames AD, Xu X, Grizzle JW, Tabuada P. Control barrier function based quadratic programs for safety critical systems. IEEE Transactions on Automatic Control 2016; 62 (8): 3861-3876.